HHS Public Access

Author manuscript

Biomech Model Mechanobiol. Author manuscript; available in PMC 2021 October 01.

Published in final edited form as:

Biomech Model Mechanobiol. 2020 October ; 19(5): 1509–1521. doi:10.1007/s10237-019-01284-5.

Mechanochemical Coupling of Formin-induced Actin Interaction at the Level of Single Molecular Complex

Zhenhai Li[1,2,*], **Hyunjung Lee**[1,*], **Suzanne G. Eskin**[1], **Shoichiro Ono**[3,‡], **Cheng Zhu**[1,4,‡], **Larry V. McIntire**[1,‡]

[1]Wallace H Coulter Department of Biomedical Engineering, Georgia Institute of Technology, Atlanta, GA 30332, USA

[2]Shanghai Key Laboratory of Mechanics in Energy Engineering, Shanghai Institute of Applied Mathematics and Mechanics, School of Mechanics and Engineering Science, Shanghai University, Shanghai, 200072, China

[3]Department of Pathology, Emory University, Atlanta, GA 30322, USA

[4]George W Woodruff School of Mechanical Engineering, Georgia Institute of Technology, Atlanta, GA 30332, USA

Abstract

Formins promote actin assembly and are involved in force-dependent cytoskeletal remodeling. However, how force alters the formin functions still needs to be investigated. Here, using atomic force microscopy and biomembrane force probe, we investigated how mechanical force affects formin-mediated actin interactions at the level of single molecular complexes. The biophysical parameters of G-actin/G-actin (GG) or G-actin/F-actin (GF) interactions were measured under force loading in the absence or presence of two C-terminal fragments of the mouse formin mDia1: mDia1Ct that contains formin homology 2 domain (FH2) and diaphanous autoregulatory domain (DAD) and mDia1Ct-ΔDAD that contains only FH2. Under force-free conditions, neither association nor dissociation kinetics of GG- and GF-interactions were significantly affected by mDia1Ct or mDia1Ct-ΔDAD. Under tensile forces (0-7 pN), the average lifetimes of these bonds were prolonged and molecular complexes were stiffened in the presence of mDia1Ct, indicating mDia1Ct association kinetically stabilizes and mechanically strengthens bonds of the dimer and at the end of the F-actin under force. Interestingly, mDia1Ct-ΔDAD prolonged the lifetime of GF- but not GG-bond under force, suggesting the DAD domain is critical for mDia1Ct to strengthen GG interaction. These data unravel the mechano-chemical coupling in formin-induced actin

‡To whom correspondence should be addressed: Prof. Larry V. McIntire, Department of Biomedical Engineering, Georgia Institute of Technology, 313 Ferst Drive NW, Atlanta, Georgia 30332, Telephone: (404) 894-5057; FAX: (404) 385-5028; larry.mcintire@bme.gatech.edu or Prof. Cheng Zhu, Department of Biomedical Engineering, Georgia Institute of Technology, 315 Ferst Drive NW, Atlanta, Georgia 30332, Telephone: (404) 894-3269; FAX: (404) 385-8109; cheng.zhu@bme.gatech.edu or Prof. Shoichiro Ono, Department of Pathology, Emory University, Atlanta, GA 30322 sono@emory.edu, Telephone: (404) 727-3916, FAX: (404)-727-8538.

*Co-first authors.

assembly and provide evidence to understand the initiation of formin-mediated actin elongation and nucleation.

Keywords

formin; actin; mechanotransduction; atomic force microscopy (AFM); single-molecule biophysics

Introduction

The actin cytoskeleton, a force-bearing and -generating structure of the cell, undergoes dynamic force loading, such as shear, tensile or compressive forces, and rearrangement during many cellular functions [1]. For example, actin filaments experience tension in stress fibers, cortex , contractile ring and compression in filopodia and lamellipodia in a range of forces, from less than 1 pN up to 100 pN per filament, and formin, mDia1, is a key player to control those actin networks [2]. Formins are the major actin binding proteins which are widely expressed in eukaryotes [3]. They play important roles in regulating actin dynamics by promoting actin nucleation and accelerating elongation while protecting the growing barbed end of F-actin from other capping proteins [3] [4-8].

Mouse mDia1 is a member of the Diaphanous formin subfamily (Dia) [4, 5] and contains regulatory and actin-binding regions (Fig. 1A). The actin-binding region facilitates actin polymerization while the regulatory region modulates formin activity by a conformational autoinhibition. The actin-binding region mainly consists of Formin Homology 1 (FH1) and FH2 domains near the C-terminal. The FH2 is the most conserved domain among formins. A flexibly tethered FH2 dimer [9] caps the barbed end of F-actin with high affinity [10, 11] The proline-rich FH1 domain recruits actin monomers through the interaction between the actin monomer-profilin complex and polyproline residues [6, 12]. The regulatory region consists of an N-terminal Diaphanous inhibitory domain (DID) and a C-terminal Diaphanous-autoregulatory domain (DAD), which form an autoinhibited conformation through interdomain interactions. The DAD also recruits actin monomers to F-actin barbed end and accelerates actin elongation [13].

Mechanochemical coupling has been observed in biomolecular motors and adhesion complexes [14]. Biochemical kinetics of actin and some of the actin binding proteins exhibit force-regulated behaviors. Mechanical force or ligand binding to F-actin can change the mechanical properties of F-actin or/and affect its binding affinity and kinetics for other actin binding proteins [15, 16]. Single-molecule experiments have demonstrated that actin depolymerization kinetics is regulated by force [17, 18]. Mechanical force also plays critical roles in formin activation and function *in vivo* [19]. Shear force applied to the cell surface is sufficient to induce mDia1 activation and increase actin polymerization, regardless of calcium or kinase signaling. However, a single molecule study using atomic force microscopy (AFM) in a range of 5~30 pN tensile forces suggested that the bond lifetimes of G-actin and F-actin(GF) interactions decreases as force increases in the presence of mDia1 C-terminal (mDiaCt; containing FH2 and DAD domains) [20]. These results are apparently

conflicting, and the mechanisms underlying how formins are activated in a force-dependent manner to facilitate actin assembly have not been fully elucidated [21].

In this study, we examined effects of low forces in a range of 0-7 pN on actin-actin interactions in the presence or absence of mDia1Ct to investigate mechanical regulation of formin-mediated actin interactions and formin/actin interactions at the level of single molecular complexes using AFM and biomembrane force probe (BFP). We also examined effects of DAD by removing DAD from mDia1Ct (Fig. 1A) because the role of this domain in the force-dependent regulation of formin has not been characterized. All the data together indicate that force facilitates formin-mediated G-actin dimerization and association to F-actin, which could be the biophysical basis for the force-dependent enhancement of the formin functions.

MATERIALS AND METHODS

BFP experimental procedure

Most of measurements in the force-free condition and low-force range (0-7 pN) were conducted using BFP, the experimental procedure of which had been described [22-24]. Briefly, two micropipettes were held oppositely on two sides of a working chamber. A biotinylated red blood cell was aspirated by the micropipette on one side. A probe glass bead pre-coated with streptavidin was attached to the apex of the red blood cell through biotin-streptavidin interaction, as tAnother glass bead, termed the target bead, was aspirated by the micropipette on the other side. The proteins of interest were captured by streptavidin on beads, respectively (Fig. 1B). Two beads were aligned and observed with an inverted microscope (a 40×/NA 0.75 objective plus a 4× television tube; Axiovert 100; Carl Zeiss) through two cameras at room temperature. One camera (CCD-100; Dage-MTI) captured real-time images at a regular video rate (30 frames per second [fps]). The other camera (GE680; Prosilica) had a high speed (1,600 fps) when the images were limited to a 30-line strip across the bead, which allowed a custom image analysis LabVIEW (National Instruments) program to track the bead position with a 3-nm (SD) displacement precision [25]. The experiment was performed in one of two modes: adhesion frequency and force-clamp. Both were conducted by repetitive contacts between the interacting molecules. The adhesion frequency assay measures force-free kinetics of protein interaction, while the force-clamp assay measures bond lifetime under at a given force [26]. In the adhesion frequency experiment, the target bead was brought to the probe bead to make contact to allow bond formation between the molecules on the two beads. After a certain contact time, the target bead was retreated to observe if it was bound to the other bead by a bond(s) or not. With 50 repeated cycles, one can numerate the frequency for binding events under the given contact time. Similarly, in the force-clamp mode, the target bead was also brought to the probe bead to make contact, then retreated. In this mode, the contact time was 0.8 s, and the coating density was adjusted to keep the adhesion frequency <20%, so that the measured adhesions were dominated by single-bond events [27]. If a bond forms, the target bead will be retreated until the force has reached a desired level and constantly clamped at the given force. A force drops to zero indicates bond dissociation and the period between start of force-clamp and the bond rupture was measured as the bond lifetime.

G-actin or biotinylated G-actin was suspended in G-buffer (5 mM Tris-HCl, 0.2 mM $CaCl_2$, 0.2 mM ATP, 0.5 mM DTT), incubated on ice for 1 h to depolymerize actin oligomers formed during storage, and centrifuged at 100k g for 1 h. The supernatants were used in the subsequent experiments.

Streptavidin conjugated beads were incubated with 4 μM of biotinylated G-actin for 1 hour, washed with G-buffer and incubated with 10 nM of biotin to block the remaining un-occupied streptavidin. One bead was attached to the apex of the micropipette-aspirated red blood cell to form a force probe and another bead was captured by the micropipette on the opposite side, which was controlled by a piezo in three directions (Fig. 1B). To prepare F-actin for GF interaction, 4 μM G-actin mixed in a 1:20 ratio of biotinylated G-actin to unlabeled G-actin were polymerized in F-buffer (50 mM KCl, 2 mM $MgCl_2$ and 1 mM ATP in G-buffer) for 15 min at room temperature followed by 1 min sonication (repetition of 5-s on and 5-s off) in an ice-water bath for three times. Experiments were conducted in the working solution (F-buffer, 1% BSA) with or without 20 nM of formin construct after 30 min preincubation. 2 uM Tmod3 was used to block the pointed end.

AFM experimental procedure

Measurements in the range of 4-25 pN force (Fig.5A) were conducted by custom-made AFM (Fig. 1C) as described in the previous studies [17, 22]. The cantilever tip we used is the long rectangular tip of OBL-10 from Bruker (Bruker inc, Billerica, MA). The spring constant of each tip were in the range of (3-12 pN/nm) and calibrated in situ by thermal fluctuation analysis. The cantilever and the petri dish were coated with biotinylated BSA, then with streptavidin, and 1 μM of biotinylated G-actin or F-actin as described above. Experiments were conducted in the working solution containing 10 nM of biotin with or without 20 nM each of formin and Tmod3.

Kinetic analysis and model fitting

The adhesion frequency P_a, measured from ≥3 samples per contact time t_c over a range of contact times was fitted by nonlinear regression to a probabilistic kinetic model for single-step monovalent receptor–ligand interaction [25, 27]

$$P_a = 1 - \exp(-\langle n \rangle) \tag{1a}$$

$$\langle n \rangle = m_r m_l A_c K_a \left[1 - \exp\left(-k_{off}^0 t_c\right)\right] \tag{1b}$$

where m_r and m_l denote the densities of the receptors and ligands, respectively, A_c is the contact area, K_a is the 2D binding affinity, and k_{off}^0 is the off-rate. We used 2 μm diameter of microbeads and applied the same impinging force for all experimental conditions, therefore, it is reasonable to assume the contact areas between two beads as a constant value in the equation. Thus, we didn't calculate the contact area, but group A_c and K_a as one parameter, an effective on-rates, A_cK_a. we used the joint parameter A_cK_a instead of K_a alone to compare the kinetics among different conditions. The superscript 0 indicates that the off-rate is evaluated at zero force to distinguish those obtained from bond lifetime measurements under force. The off-rate was obtained by fitting bond lifetime distribution.

Molecular stiffness analysis

Determination of the stiffness of a molecular bond has been previously described [23, 28, 29]. Briefly, it is measured from the force-ramp phase of the BFP test cycles. The loading rate was preset at 1000 pN/s, which can be translated to a displacement speed of 333.3 nm/s. The force vs. displacement curve is obtained eliminating time from the force vs. time data from the bead tracking system and from the displacement vs. time data from the piezoelectric actuator capacitance sensor feedback system. A straight line was fit to tensile force segment of this linear data to obtain the slope, which represents the stiffness of the molecular complex linking the two glass beads, k_m. An ensemble of k_m values were analyzed by histograms and fitted by single or double Gaussian distributions (Fig. 4). The extra sum-of-squares F test was used to determine whether the single Gaussian or double Gaussian is a better fit.

Two-state fitting

The two-state model used here has been described by previous studies [22]. Briefly, the survival frequency is assumed to be a superposition of two exponential decays as

$$\ln(\text{Survival Frequency}) = \ln[\omega_1 \exp(-k_1 t) + \omega_2 \exp(-k_2 t)]$$

The parameters of ω_i and k_i are occupancy and off-rate of the ith state, $i = 1$ and 2 for the short- and long-lived states, respectively, which satisfies $\omega_1 + \omega_2 = 1$. For each distribution, data were first fitted by a single exponential decay. If the R-square is less than 0.95, the two-state fitting was used as shown in Fig. S1 and Table 1.

Protein preparation

G-actin and biotinylated G-actin were purchased from Cytoskeleton Inc. and prepared according to manufacturer's instruction and previous studies [17, 30]. The mDia1Ct construct (residues 748-1203) in pGEX-KT, which contains FH2 and DAD but not FH1 domain, was provided by Dr. Henry N. Higgs (Dartmouth Medical School), expressed in *E. coli* Rosetta2 and purified as described previously [31] . Briefly, The *E. coli* was grown to OD600 0.6-0.8 in LB with 100 μg/ml ampicillin and 34 μg/ml chloramphenicol at 37 °C, then the culture was cooled down to 16 °C, added 0.5 mM IPTG and continued to grow overnight. The culture was centrifuged, resuspended in EB (50 mM Tris-HCl pH8, 500 mM NaCl, 5 mM EDTA, 1 mM DTT and 1 pill/50ml complete protease inhibitor), then sonicated and ultracentrifuged. The supernatant was loaded on glutathione-Sepharose 4B and washed with WB (5 mM Tris-HCl pH8, 250 mM NaCl, 0.05 mM EDTA, 1 mM DTT and 0.1% Thesit). The 50% slurry of beads was added with 10 U/ml thrombin to cleave GST-tag, and then cleaved mDia1Ct was eluted from the column. 1 mM PMSF was added to stop thrombin activation and the eluate was dialyzed against the buffer (2 mM $NaPO_4$pH 7, 150 NaCl, 0.1 mM EGTA, 0.5 mM DTT) and stored at −20 °C with glycerol.

The expression vector for mDia1Ct-ΔDAD (residues 748-1179) was made by introducing a stop codon (TGA) in pGEX-mDia1Ct by a QuickChange Site-Directed Mutagenesis kit

(Agilent Technologies). The recombinant mDia1Ct-ΔDAD protein was expressed and purified essentially in the same manner as mDia1Ct.

Tmod3 was bacterially expressed using the expression vector (provided by Dr. Velia Fowler, The University of Delaware) and purified as described previously [32].

Flow cytometry

Beads coated with G-actin or F-actin were respectively incubated with mDia1Ct for 1 h at room temperature, washed 3 times with G-buffer plus 1% BSA, incubated with goat anti-G-actin mAh PA5-19033 (from Thermo Scientific Inc, IL USA) for 30 min and washed 3 times. It was followed by incubation with respective PE conjugated rabbit-anti-goat antibody at room temperature for 30 min, wash with G-buffer plus 1% BSA, and analysis by a BD LSR flow cytometer (BD). The number of molecules per bead was determined from the fluorescence intensity after calibration by standard beads (BD Quantibrite PE Beads). The site density was obtained by dividing the total number of molecules by the surface area of the bead.

RESULTS

In this study, two force microscopies were used, biomembrane force probe (BFP) and AFM, to measure piconewton unit of force. Measurements in the force-free condition and low-force range (0-7 pN) were conducted using BFP (Fig. 1B), and measurements in the range of 4-25 pN force were by custom-made AFM (Fig. 1C).The principle of BFP is using a pretreated red blood cell as a force transducer to measure the force on a single molecule or a single molecule complex. Two micropipettes are used, one to hold a red blood cell with a glass bead attaching to its apex and the other one to hold a bead presenting or coated with the molecule of interests. he mechanical properties of red blood cell are well characterized, so it is widely used as a mechanical probe [25, 29]. AFM uses a microfabricated cantilever as a force transducer to measure forces loaded between the tip of the cantilever and the sample. We immobilized G-actin and/or F-actin on streptavidin-coated glass beads for BFP experiments or streptavidin-coated cantilever tip and polystyrene petri dish surface for AFM experiments (Fig. 1B and C; details in Experimental Procedures). 2 uM Tmod3 was added to cap the pointed end to examine actin interaction at the barbed end. In some experiments, one of the formin constructs, mDia1Ct or mDia1Ct-ΔDAD, was added 30 min prior to the measurements. Three types of biophysical data were collected from repeated contacts of the two interacting molecules: force-free kinetics quantified from the adhesion frequency assay [25, 27], bond lifetime measured under a force-clamping mode [25], and molecular stiffness estimated from the slope of the force ramping phase [27] (Fig. 2A, 3A and 4A; see Molecular stiffness analysis).

Limited effects of formin mDia1Ct on the kinetics of G-actin/G-actin and G-actin/F-actin interaction under force-free conditions

We first tested the effect of the formin fragments on actin assembly kinetics by measuring the effective on-rates and off-rates of GG and GF interactions in the absence or presence of either formin construct under a force-free condition using the adhesion frequency assay by

BFP. Typically, adhesion frequency increases as contact time (the duration of contact between two functionalized surfaces; the width of green traces in Fig. 2A) increases, and reaches a plateau after a certain contact time as shown in Fig. 1D-G. Fitting the adhesion frequency vs. contact time curve to a probabilistic kinetic model yielded two parameters: the product of effective on-rates and molecular densities ($m_r m_1 A_C k_{on}$) and the off-rates (k_{off}) [25, 27] (Fig. 2B to G; details in Experimental Procedures). Note that measuring the molecular density in the AFM setup is technically difficult. To ensure consistency of densities of the coated molecules (G-actin and F-actin) in experiments assessing the effects of formin, we performed the experiments with or without mDia1Ct constructs side-by-side. Therefore, the differences in $m_r m_1 A_C k_{on}$ can be attributed to the differences in effective on-rates.

Both formin constructs do not contain the FH1 domain, which effectively recruits profilin-G-actin complexes to the barbed end [7]. Thus, as expected, no significant effects of both the soluble formin constructs were detected by comparing the adhesion curves (Fig. 1D to G) and the fitted parameters (Fig. 2B and 2C). Besides adhesion frequency assay, off- and on-rates were also measured by monitoring thermal fluctuations without applied force on the actin bonds [25, 33]. The zero-force lifetimes of GG and GF interaction measured from thermal fluctuation assay showed no difference with and without mDia1Ct (Fig. S1A and S1B).

The measured force-free off-rates by adhesion frequency assay were 2.25±0.18 s^{-1}, 1.94±0.63 s^{-1}, and 2.94±0.83 s^{-1} for GG interaction in the absence and presence of mDia1Ct-ΔDAD or mDia1Ct, respectively. The values for GF interactions in the absence and presence of mDia1Ct were 1.71±0.61 s^{-1} or 1.59±0.46 s^{-1}, respectively (Figure 2C). Thus, the mDia1Ct and mDia1Ct-ΔDAD constructs have limited effects on either the association or dissociation kinetics of GG and GF interaction under force-free conditions.

Dissociation kinetics of mDia1Ct-mediated actin interactions are regulated by force

To investigate force regulation in formin-mediated actin interactions, the lifetimes of GG and GF interactions were measured in a range of low forces using a force clamping mode by BFP (Fig. 3A; 0-5 pN for GG and 0-7 pN for GF). In contrast to force-free dissociation kinetics, the force-dependent bond lifetimes (reciprocal off-rates) of these actin interactions were significantly impacted by the addition of formin constructs. In the presence of mDia1Ct, both GG and GF interactions behaved as catch bonds in which the lifetime is prolonged by increasing force (Fig. 3B and 3C, red squares), whereas in the absence of mDia1Ct, both interactions exhibited an ideal bond characteristic in which the lifetime was indifferent to force, at ~0.4 s or ~0.5 s for GG or GF interaction, respectively (Fig. 3B and 3C, black circles). Interestingly, the mDia1Ct-ΔDAD construct also converted the GF interaction from an ideal bond to a catch bond indistinguishable from that of GF interaction in the presence of mDia1Ct, but did not affect the GG interaction (Fig. 3B and 3C, blue diamonds; see Tables S2 and S3 for the unpaired Student's t-test results of lifetime at different force), indicating the DAD domain is required to stabilize the GG interaction under force.

We further examined lifetime distributions to gain insight into the catch bond characteristics of the GG and GF interaction in the presence of mDia1Ct. The lifetime distributions of GG and GF interactions showed nearly single exponential decays under the lowest forces (1-2 pN, Fig. S1C and S1F, black circles). Force had relatively small impact on the bond lifetime distributions of GG interactions in the absence of formin (Fig. S1C, red squares). By comparison, the bond distributions of GG and GF interactions in the presence of mDia1Ct changed to a clear superposition of two exponential decays at higher forces (Fig. S1D and S1G, red squares and blue triangles). Interestingly, the presence of mDia1Ct-ΔDAD impacted the bond lifetime distributions of GF but not GG interactions (Fig. S1E and S1H, red squares and blue triangles). The double exponential decays suggest that actin bonds were dissociated from two states (long- and short-lived states) [34] and/or through two pathways (slow- and fast-pathways) [35].

We thus compared the goodness-of-fit of the single-state and two-state models to fit the lifetime distributions (details in Experimental Procedures). The best-fit off-rates and occupancies of the two models and the statistics comparing their goodness-of-fits are summarized in Table 1. In the presence of mDia1Ct, the fraction of the long-lived state (α) of the GG interaction increased from 0 in the absence of mDia1Ct to 30% as force increased (Fig. S1D and Table 1). In addition, the off-rate of the long-lived state (k_2) decreased as force increased (Fig. S1D and Table 1). As a result of both effects, the average lifetime was prolonged as force increased. For the GF interaction, force induced the long-lived state and mDia1Ct association further promoted the long-lived state from 18% to over 30% (Fig. S1F and S1G, Table 1). The mDia1Ct-ΔDAD construct had a similar effect on the best-fit parameters of the GF interaction as the mDia1Ct had, but had negligible effect on those of the GG interaction (Fig. S1E and S1H).

mDia1Ct binding modulates mechanical properties of the actin bonds

In our BFP setup, molecular bonds were formed by contacting the two glass beads, as described in the Materials and Methods. As tensile force was applied upon the molecular bond, the molecular complex was extended, like a spring extension by force loading, and the extension can be measured on the time-force trace. The stiffness of the bond can be derived from the force and extension. Molecular stiffness measurement has been proved to be valuable in examining subtle differences of proteins, such as integrins and selectins, in single-molecule experiments [23, 36, 37]. Force on or ligand binding to F-actin affects its affinities for other actin-binding proteins [15, 16] and changes its mechanical properties [38, 39]. Therefore, we investigated whether mDia1Ct binding affects the stiffness (spring constant) of the molecular complex containing a GG or GF bond. The stiffness was measured from the slope of the force-time trace of the loading ramp by BFP (Fig. 4A, details in Experimental Procedure) [28].

The spring constants of the actin bonds follow single peak Gaussian distributions, with averages of 0.21±0.17 and 0.25±0.12 pN/nm for GG and GF, respectively (open black bars in Fig. 4B and 4C). When mDia1Ct was added, a second peak of a higher mean value emerged in the spring constant distribution for the GG interaction (striped gray bars in Fig. 4B). This distribution was fitted by a double Gaussian distribution, returning an average

spring constant of 0.80±0.11 pN/nm and a ~40 % of population under the second peak. The spring constant of the GF interaction in the presence of mDia1Ct displayed a single peak with a broader and right-shifted distribution peaked at a higher mean value of 34±0.22 pN/nm (Fig. 4C). These data suggest that formin association to the actin dimer or the F-actin stiffens the actin-actin bonds.

Formin-actin interactions also exhibit force-regulated characteristics

To further investigate the detailed mechanism underlying the formin-mediated actin interaction, we examined interactions between each mDia1Ct fragment and G-actin or F-actin using AFM. Formin constructs and actin were coated on the AFM cantilever tips and polystyrene surfaces, respectively. The effective on-rate of mDia1Ct/G-actin interaction was obtained by adhesion frequency measurements and force-dependent lifetimes of bonds of mDia1Ct or mDia1Ct-ΔDAD with F-actin or G-actin were measured by AFM using force-clamp.

The mDia1Ct/F-actin and mDia1Ct-ΔDAD/F-actin interactions exhibited indistinguishable slip bonds where bond lifetime decreased as force increased in the range of 5 – 20 pN (Fig. 5A and Fig. S4; see Table S5 for the unpaired Student's t-test results of lifetime at different force). In addition, the mDia1Ct/F-actin bond persisted more than 1 hour under force-free conditions as assessed by flow cytometry (Fig. S6). Such an interaction is too long to be tested by AFM or BFP measurement, owing to the drift of the system, the survival time of red blood cell in BFP, and the low throughput of these techniques. These data indicate that mDia1Ct in the experimental buffer stably binds to the F-actin, consistent with other studies showing formin capping the barbed end of F-actin [40, 41].

In contrast to the mDia1Ct/F-actin interaction, mDia1Ct/G-actin interaction exhibited an ideal bond behavior with much shorter (<0.5 s) average bond lifetimes compared to those of the mDia1Ct/F-actin or mDia1Ct-ΔDAD/F-actin interactions (Fig. 5A and Fig. S4; $p<0.05$ with unpaired Student's t-test between the average bond lifetimes at different forces in Table S5). These values are comparable to those of GG interaction in the absence of mDia1Ct, but significantly ($p<0.01$ with the Student's t-test) shorter than those of mDia1Ct-mediated GG interaction under 5 pN of force (Fig. 3B). The force-free mDia1Ct/G-actin off-rate was ~1.8 s^{-1} (Fig. 5B), comparable to the off-rates of GG interactions (Fig. 2C). In addition, the adhesion frequency of the mDia1Ct-ΔDAD construct with G-actin was negligibly low, 2.8±1.4 % at 0.8 s contact time (Fig. 5B, gray square), consistent with our observation that mDia1Ct-ΔDAD had undetectable effect on GG interaction (Fig. 3B). The differential adhesion frequencies between the two formin constructs suggest that the DAD domain strengthens the interaction between mDia1Ct and G-actin.

To further investigate the effect of formin on actin dimerization, we measured the stability under a 5 pN force of GG bonds formed with different contact times (the width of green traces in Fig. 2A) in the presence of mDia1Ct. Two different contact times, 0.1 s for a short and 2 s for a steady-state contact time, were chosen based on the adhesion frequency versus contact time curve of the GG interaction (Fig. 1D). The average lifetimes were 0.55 and 0.81 s for the 0.1- and 2-s contact times, respectively (Fig. 5C, open bars), and for both contact time the lifetime distributions followed double exponential decays (Fig. 5D). It seemed

reasonable to assume that different contact times do not affect the short- and long-lived off-rates, we therefore fitted the bond lifetime distributions by the two-state model with the constraints that the corresponding off-rates in the two distributions were the same but the fractions of the short- and long-lived bonds might differ. We estimated the fractions of the long-lived bonds, which increased from ~20% at 0.1-s contact time to ~45% at 2-s contact time (Fig. 5C, striped gray bars). The best-fit off-rates of the short- and long-lived states were 2.76 s^{-1} and 0.68 s^{-1}, respectively. The short-lived state off-rate was comparable to that of GG interaction in the absence of mDia1Ct, suggesting the short-lived bonds are from GG interaction alone. The long-lived bonds may be induced by mDia1Ct together with mechanical force. The long contact time resulted in a larger fraction of long-lived bonds, possibly because longer contact time provided more chance for actin to form a dimer, and the dimer, in turn, promoted the association with mDia1Ct. This proposition is supported by the force-lifetime measurement with a 0.8 s contact time (used in Fig. 3), which produced the long-lived state fraction of ~30%.

DISCUSSION

In this single-molecular complex study, we demonstrated that mDia1Ct-mediated actin interactions were modulated when tensile forces (1 – 7 pN) were applied to the actin bonds. Both the bonds in the G-actin dimer and at the barbed end of F-actin were mechanically strengthened in the presence of mDia1Ct. Mechanical force further prolonged the lifetime of these bonds. The mechanical and kinetic modifications are coupled to regulate formin-mediated actin dynamics. Based on our findings, here, we consider several possible models for formin-mediated actin interactions. Based on our data, we exclude the less likely model and propose two more favorable models below for formin-mediated GG and GF interactions, respectively.

Considering that the FH2 domain tightly binds to the barbed end of F-actin and that DAD domain binds to actin monomers [33, 34], there are two possible models for mDia1Ct-mediated GG interaction: 1) serial molecular interaction (SMI) model and 2) compact tetramolecular complex (CTC) model. In the SMI model, the two DAD domains on the mDia1Ct dimer recruit two G-actin monomers respectively, forming a G-actin–mDia1Ct–G-actin bond as serial linkages (Fig. 6A left). In the CTC model, two G-actins spontaneously dimerize before binding to formin. The mDia1Ct dimer then embraces the G-actin dimer, forming a compact tetramolecular complex to stabilize the G-actin dimer. (Fig. 6A right).

We propose that the CTC model is a more likely mechanism rather than the SMI for the assembly of the initial stage of mDia1Ct-mediated actin nucleation, based on the following findings in this study. First, the significantly longer lifetime of GG bonds under tensile forces in the presence of mDia1Ct and also that of mDia1Ct/G-actin bond lifetimes: in the SMI model, the off-rate measurements are expected to be mostly from dissociation of the weakest molecular pair in the linkage. In contrast, the off-rate in the CTC model would be mostly from G-actin/G-actin bond, which is embraced by DAD domains. The significantly enhanced bond lifetimes rule out the SMI model. Second, the comparable on-rates of GG interaction in the presence and absence of mDia1Ct: the FH2–FH2 are pre-formed in the solution, thus, the on-rate of the SMI model would be measured from the on-rate between

the DAD domain and G-actin. If the CTC model is correct, the on-rate is expected to be comparable to that of GG interaction. Therefore, the on-rate measurements support the CTC model. Third, the contact-time dependence of GG interaction in the presence of mDia1Ct: longer bond lifetime of GG with longer contact time suggests that mDia1Ct has more chance to interact with GG during the contact, resulting in stabilization of the actin-formin complex (CTC model).

In our experimental setup, it is difficult to determine which domains of mDia1Ct are involved in G-actin dimer/mDia1Ct binding. Nevertheless, if we introduce mutations at the possible binding domain on the FH2 or DAD, the tetramolecular complex will be less compact or/and the formin-mediated nucleation will be inhibited. In addition, using monomeric mDia1Ct or constructs consisting only of the DAD domains would reveal further information about how mDia1Ct interacts with G-actin dimer and how it promotes the early stage of nucleation.

The mDia1Ct association with the actin dimer will help overcome kinetic barriers of short-lived intermediates (dimer and trimer) to form a tetramer, a stable seed for polymerization [42]. This concept, capturing and stabilizing the spontaneously formed dimer, has been proposed [43], but a weak point of this model has been the lack of FH2 binding to the actin monomer *in vitro*. However, recent studies have shown that the C-terminal DAD domain binds the actin monomer [44, 45]. In this study, we observed the binding of G-actin monomer to mDia1Ct but not to mDia1Ct-ΔDAD, confirming that the DAD domain is required for formin C-terminal interaction with G-actin. Moreover, in the presence of mDia1Ct, the G-actin dimer can be stabilized by a small tensile force, ~3 pN, compared to the force-free condition. In contrast, mDia1Ct-ΔDAD has no significant effect on GG interaction, indicating that the DAD domain is required for the stabilization of the GG interaction (Fig. 3B). Thus, the initial stage of formin-mediated actin nucleation could be that G-actin forms a dimer first, and mDia1Ct embraces the dimer through DAD and actin dimer interaction and reinforces the interaction (Fig. 6A right). Force can further stabilize mDia1Ct-mediated G/G interaction. The stabilized actin dimer would further facilitate the association of another G-actin monomer to form a trimer.

Similarly, there are also two possible interaction models for the mDia1Ct-mediated GF interaction: one is a G-actin–formin–F-actin serial bond (Fig. 6B left) and the other is a compact complex of G-actin/mDia1Ct-dimer/F-actin (Fig. 6B right). The bond lifetime of mDia1Ct-mediated GF bond is significantly longer than that of mDia1Ct/G-actin interaction. Therefore, the lifetime measured in the presence of mDia1Ct is not from a serial bond, but a compact complex of G-actin/mDia1Ct-dimer/F-actin, which is a widely accepted model. It is worth noting that, although DAD is required to mediate GG interaction, it has no effect on GF interaction.

Full-length formin, forming an autoinhibited conformation through interdomain interactions between the N-terminal DID and C-terminal DAD, needs to be activated to accelerate actin nucleation or elongation in physiological conditions [4]. Actin nucleation is inhibited in the presence of N-terminal construct containing the DID and the full C-terminus of mDia1 [46], in addition, autoinhibition by DAD/DID interaction is only partially activated through RhoA

binding to the GTPase-binding domain on the N-terminal in the full-length formin and the N-/C- terminal fragments *in vitro* [13, 31]. Therefore, several possibilities have been proposed to fill the missing link of full activaiton, such as local concentration of G-actin and existence of co-factors or nucleation promoting factors [4, 47]. As formins localize to sites of mechanotransduction [21, 48], we speculate that mechanical force might serve as a nucleation co-factor to facilitate efficient activation of formin and promote actin assembly. One possible mechanism would be that force induces dissociation of the DAD/DID interaction (Fig. 6C). But additional experiments are needed to test this model. Our study demonstrated that tensile force significantly prolongs the lifetime of formin-mediated GF interaction, suggesting force may facilitate actin assembly in adhesion complexes. As GG and GF interactions closely mimic actin dimerization and the G-actin monomer association at the end of F-actin respectively, our results suggest that force and formin together facilitate actin nucleation and elongation.

GG and GF interactions were known to exhibit a biphasic catch-slip behavior under force loading condition, in which the lifetime first increases with force increasing, after reaching the peak, the lifetime decreasing with force increasing [17]. This study showed the bond lifetime peaks were at ~ 10 pN for GG and ~20 pN for GF interaction [17]. Later another single-molecular study, which performed under a force range of 5 ~ 30 pN using AFM in the presence of mDia1Ct, showed that bond lifetimes of GG and GF interaction decreased as force increased, so called a slip bond behavior [20]. By using BFP with a much softer force transducer, we were able to explore the force-regulated GG and GF interaction in a force range of 0 ~ 7 pN, and found that GG and GF interactions exhibited a catch bond behavior in the presence of mDia1Ct, where the bond lifetimes increased as force increased. Jégou *el al.* showed a similar result that actin elongation rate significantly increased by formin, when actin filament was pulled by 0 ~ 3.5 pN of forces [18]. These findings suggest that GG and GF interactions in the presence of mDia1Ct t still behave as catch-slip, but the peaks of bond lifetime were lowered to ~5 pN for GG interaction and ~ 7 pN for GF interaction comparing to those in the absence of mDiaCt.

In our experimental setup, association and dissociation kinetics of both GG and GF bonds were not significantly affected by mDia1Ct alone under force-free conditions. The force-free kinetics of GF interaction are consistent with the study by Kovar *et al.*, which demonstrated that, in the absence of profilin, mDia1Ct elongates the barbed end at the same rate as that without formin [10]. The comparable on-rates of GF interaction in the presence and absence of formin indicate that mDia1Ct neither blocks nor promotes G-actin association at the barbed end. In addition, we had examined different concentrations of mDia1Ct (2.5 – 10 nM) [30]. mDia1Ct concentrations higher than 5 nM showed no impact on GG and GF interaction kinetics (data not shown). Thus, the concentration of mDia1Ct higher than 5 nM could be considered as a saturation concentration. An over saturated concentration, 20 nM of mDia1Ct was used in this study to secure the actins are all occupied by mDia1Ct in the experiments.

Bugyi *et al.*[49] and Papp *et al.*[50] showed that flexibility of F-actin increases and that interactions between neighboring actin subunits are weakened in the presence of mDia1-FH2. Their time-resolved fluorescence anisotorpy experimental setup allowed to observe

that the effect of formin binding to the barded end propagates along the filament. However, our experiment setup measures the force, stiffness and bond lifetime of the most terminal molecular complex at the end of the filament. Further study to elucidate the effect of molecular stiffness or allosteric chances induced by mechanical force at the end of F-actin will add valuable information.

We have observed ~0.3-~0.5 s of bond lifetimes of GG interactions in this study and previous studies[17, 51]. The measured dissociation rates are quite different from 10^8-10^{10} per second of actin dimer dissociation [42]. Considering a previous study proposed “activated actin monomers” before the nucleation process as one of steps during actin polymerization [52]. There might be a small population of actin in the experiments are activated. It is possible that only the activated actin with long-lived interactions survive to be detected and measured under force-clamped AFM or BFP experiments, resulting in measurement of the stable actin dimers. Further we hypothesis that the minor population of the stable actin dimers could serve as “activated actin monomers”. The formin DAD domain and mechanical force could promote the activated actin monomer interactions even further to facilitate actin nucleation. The detailed biophysical mechanisms of the activated actin monomer are not clear, these actins could be pre-exist in the actin monomers with a low percentage, which can hardly be detected with bulk experiments, or they are activated by pulling in the AFM or BFP experiments. The detailed mechanism could be a direction for future study.

Supplementary Material

Refer to Web version on PubMed Central for supplementary material.

ACKNOWLEDGEMENTS

This work is supported by NIH grant R01 HL18671 to L.V.M., R01 AR048615 to S.O. and R01 AI044902 to C.Z.

REFERENCES

1. Parsons JT, Horwitz AR, and Schwartz MA, Cell adhesion: integrating cytoskeletal dynamics and cellular tension. Nat Rev Mol Cell Biol, 2010 11(9): p. 633–43. [PubMed: 20729930]
2. Zimmermann D and Kovar DR, Feeling the force: formin's role in mechanotransduction. Curr Opin Cell Biol, 2019 56: p. 130–140. [PubMed: 30639952]
3. Chesarone MA, DuPage AG, and Goode BL, Unleashing formins to remodel the actin and microtubule cytoskeletons. Nat Rev Mol Cell Biol, 2010 11(1): p. 62–74. [PubMed: 19997130]
4. Breitsprecher D and Goode BL, Formins at a glance. J Cell Sci, 2013 126(Pt 1): p. 1–7. [PubMed: 23516326]
5. Alberts AS, Diaphanous-related Formin homology proteins. Curr Biol, 2002 12(23): p. R796. [PubMed: 12477401]
6. Watanabe N, et al., p140mDia, a mammalian homolog of Drosophila diaphanous is a target protein for Rho small GTPase and is a ligand for profilin. Embo Journal, 1997 16(11): p. 3044–3056. [PubMed: 9214622]
7. Shekhar S, et al., Formin and capping protein together embrace the actin filament in a menage a trois. Nat Commun, 2015 6: p. 8730. [PubMed: 26564775]
8. Bombardier JP, et al., Single-molecule visualization of a formin-capping protein 'decision complex' at the actin filament barbed end. Nat Commun, 2015 6: p. 8707. [PubMed: 26566078]

9. Xu Y, et al., Crystal structures of a Formin Homology-2 domain reveal a tethered dimer architecture. Cell, 2004 116(5): p. 711–23. [PubMed: 15006353]
10. Kovar DR, et al., Control of the assembly of ATP- and ADP-actin by formins and profilin. Cell, 2006 124(2): p. 423–35. [PubMed: 16439214]
11. Zigmond SH, Formin-induced nucleation of actin filaments. Curr Opin Cell Biol, 2004 16(1): p. 99–105. [PubMed: 15037312]
12. Wasserman S, FH proteins as cytoskeletal organizers. Trends in Cell Biology, 1998 8(3): p. 111–115. [PubMed: 9695820]
13. Maiti S, et al., Structure and activity of full-length formin mDia1. Cytoskeleton (Hoboken), 2012 69(6): p. 393–405. [PubMed: 22605659]
14. Bao G, et al., Molecular Biomechanics: The Molecular Basis of How Forces Regulate Cellular Function. Mol Cell Biomech, 2010 3(2): p. 91–105. [PubMed: 20700472]
15. Hayakawa K, Tatsumi H, and Sokabe M, Actin filaments function as a tension sensor by tension-dependent binding of cofilin to the filament. J Cell Biol, 2011 195(5): p. 721–7. [PubMed: 22123860]
16. Uyeda TQ, et al., Stretching actin filaments within cells enhances their affinity for the myosin II motor domain. PLoS One, 2011 6(10): p. e26200. [PubMed: 22022566]
17. Lee CY, et al., Actin depolymerization under force is governed by lysine 113:glutamic acid 195-mediated catch-slip bonds. Proc Natl Acad Sci U S A, 2013 110(13): p. 5022–7. [PubMed: 23460697]
18. Jegou A, Carlier MF, and Romet-Lemonne G, Formin mDia1 senses and generates mechanical forces on actin filaments. Nat Commun, 2013 4: p. 1883. [PubMed: 23695677]
19. Higashida C, et al., F- and G-actin homeostasis regulates mechanosensitive actin nucleation by formins. Nat Cell Biol, 2013 15(4): p. 395–405. [PubMed: 23455479]
20. Lee CY, et al., Regulation of actin catch-slip bonds with a RhoA-formin module. Sci Rep, 2016 6: p. 35058. [PubMed: 27731359]
21. Leckband D, Formin' cables under stress. Nat Cell Biol, 2013 15(4): p. 345–6. [PubMed: 23548927]
22. Kong F, et al., Cyclic mechanical reinforcement of integrin-ligand interactions. Mol Cell, 2013 49(6): p. 1060–8. [PubMed: 23416109]
23. Fiore VF, et al., Dynamic catch of a Thy-1-α5β1+ syndecan-4 trimolecular complex. Nature communications, 2014 5.
24. Liu B, et al., Accumulation of dynamic catch bonds between TCR and agonist peptide-MHC triggers T cell signaling. Cell, 2014 157(2): p. 357–68. [PubMed: 24725404]
25. Chen W, et al., Measuring Receptor-Ligand Binding Kinetics on Cell Surfaces: From Adhesion Frequency to Thermal Fluctuation Methods. Cell Mol Bioeng, 2008 1(4): p. 276–288. [PubMed: 19890486]
26. Chen W, Lou J, and Zhu C, Forcing switch from short- to intermediate- and long-lived states of the alphaA domain generates LFA-1/ICAM-1 catch bonds. J Biol Chem, 2010 285(46): p. 35967–78. [PubMed: 20819952]
27. Chesla SE, Selvaraj P, and Zhu C, Measuring two-dimensional receptor-ligand binding kinetics by micropipette. Biophys J, 1998 75(3): p. 1553–72. [PubMed: 9726957]
28. Marshall BT, et al., Measuring molecular elasticity by atomic force microscope cantilever fluctuations. Biophys J, 2006 90(2): p. 681–92. [PubMed: 16258054]
29. Chen W, et al., Observing force-regulated conformational changes and ligand dissociation from a single integrin on cells. J Cell Biol, 2012 199(3): p. 497–512. [PubMed: 23109670]
30. Pankov R, et al., Integrin dynamics and matrix assembly: Tensin-dependent translocation of alpha(5)beta(1) integrins promotes early fibronectin fibrillogenesis. Journal of Cell Biology, 2000 148(5): p. 1075–1090. [PubMed: 10704455]
31. Li F and Higgs HN, The mouse Formin mDia1 is a potent actin nucleation factor regulated by autoinhibition. Curr Biol, 2003 13(15): p. 1335–40. [PubMed: 12906795]
32. Fischer RS, Fritz-Six KL, and Fowler VM, Pointed-end capping by tropomodulin3 negatively regulates endothelial cell motility. J Cell Biol, 2003 161(2): p. 371–80. [PubMed: 12707310]

33. Chen W, et al., Monitoring receptor-ligand interactions between surfaces by thermal fluctuations. Biophys J, 2008 94(2): p. 694–701. [PubMed: 17890399]
34. Fowler FJ, Six lessons from PPS. Rehab Manag, 2003 16(7): p. 18–20, 69.
35. Evans E, et al., Mechanical switching and coupling between two dissociation pathways in a P-selectin adhesion bond. Proceedings of the National Academy of Sciences of the United States of America, 2004 101(31): p. 11281–11286. [PubMed: 15277675]
36. Sarangapani KK, et al., Molecular stiffness of selectins. Journal of Biological Chemistry, 2011 286(11): p. 9567–9576. [PubMed: 21216951]
37. Chen Y, et al., An integrin α IIb β 3 intermediate affinity state mediates biomechanical platelet aggregation. Nature materials, 2019: p. 1. [PubMed: 30542100]
38. Shimozawa T and Ishiwata S, Mechanical distortion of single actin filaments induced by external force: detection by fluorescence imaging. Biophys J, 2009 96(3): p. 1036–44. [PubMed: 19186141]
39. Matsushita S, et al., Effect of tensile force on the mechanical behavior of actin filaments. J Biomech, 2011 44(9): p. 1776–81. [PubMed: 21536289]
40. Kovar DR and Pollard TD, Insertional assembly of actin filament barbed ends in association with formins produces piconewton forces. Proc Natl Acad Sci U S A, 2004 101(41): p. 14725–30. [PubMed: 15377785]
41. Pruyne D, et al., Role of formins in actin assembly: nucleation and barbed-end association. Science, 2002 297(5581): p. 612–5. [PubMed: 12052901]
42. Sept D and McCammon JA, Thermodynamics and kinetics of actin filament nucleation. Biophys J, 2001 81(2): p. 667–74. [PubMed: 11463615]
43. Pring M, et al., Mechanism of formin-induced nucleation of actin filaments. Biochemistry, 2003 42(2): p. 486–96. [PubMed: 12525176]
44. Vizcarra CL, Bor B, and Quinlan ME, The role of formin tails in actin nucleation, processive elongation, and filament bundling. J Biol Chem, 2014 289(44): p. 30602–13. [PubMed: 25246531]
45. Gould CJ, et al., The formin DAD domain plays dual roles in autoinhibition and actin nucleation. Curr Biol, 2011 21(5): p. 384–90. [PubMed: 21333540]
46. Li F and Higgs HN, Dissecting requirements for auto-inhibition of actin nucleation by the formin, mDia1. Journal of Biological Chemistry, 2005 280(8): p. 6986–6992. [PubMed: 15591319]
47. Breitsprecher D, et al., Rocket launcher mechanism of collaborative actin assembly defined by single-molecule imaging. Science, 2012 336(6085): p. 1164–8. [PubMed: 22654058]
48. Paul AS and Pollard TD, Review of the mechanism of processive actin filament elongation by formins. Cell Motil Cytoskeleton, 2009 66(8): p. 606–17. [PubMed: 19459187]
49. Bugyi B, et al., Formins regulate actin filament flexibility through long range allosteric interactions. Journal of Biological Chemistry, 2006 281(16): p. 10727–10736. [PubMed: 16490788]
50. Papp G, et al., Conformational changes in actin filaments induced by formin binding to the barbed end. Biophysical journal, 2006 91(7): p. 2564–2572. [PubMed: 16829561]
51. Lee H, et al., Force-history dependence and cyclic mechanical reinforcement of actin filaments at the single molecular level. J Cell Sci, 2019 132(4).
52. Cooper JA, et al., Kinetic evidence for a monomer activation step in actin polymerization. Biochemistry, 1983 22(9): p. 2193–202. [PubMed: 6860660]

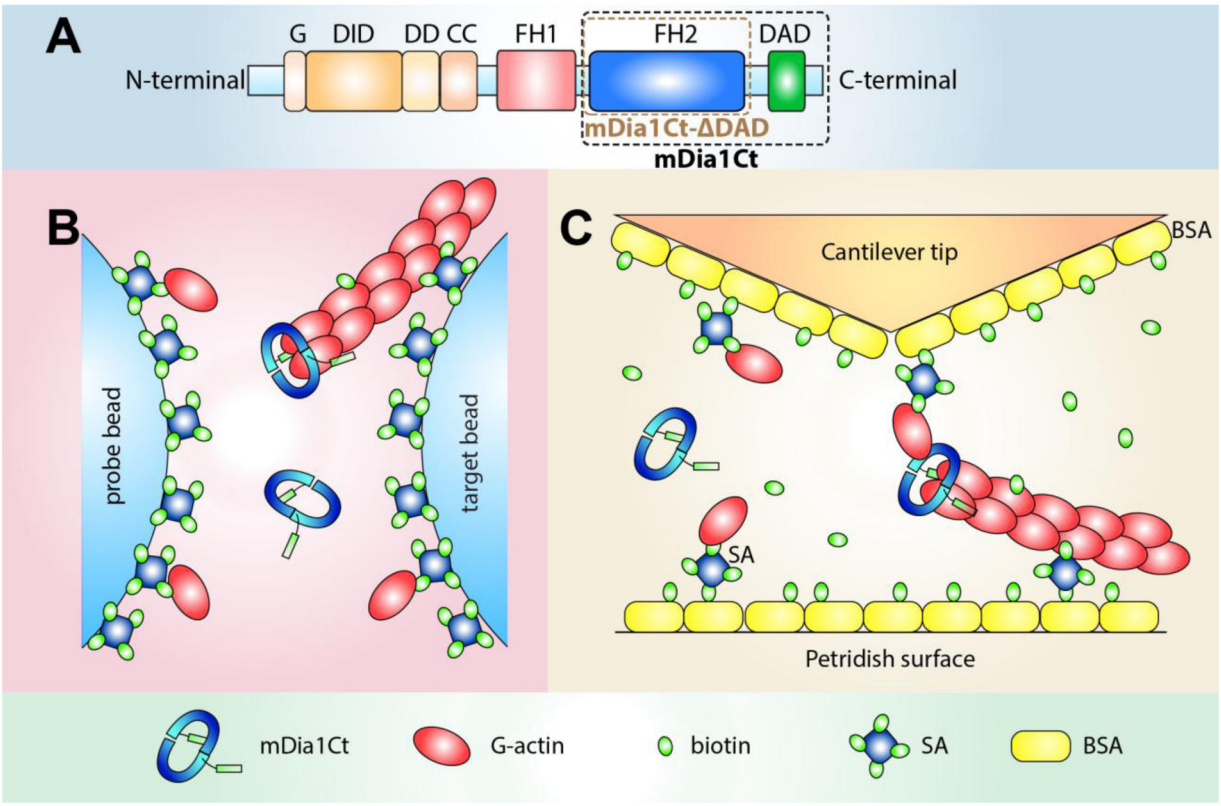

FIGURE 1.

Schematics of experiments. (A) The mDia1 constructs used in this study. The black dotted-line box contains the C-terminal region of FH2 and DAD domains (mDia1Ct) and light brown dotted-line box contains the FH2 domain (mDia1Ct-ΔDAD). (B) BFP; GG (lower) and GF (upper) interactions. The probe bead served as a force transducer and the target bead controlled the repetitive contact with 1 nm precision. For GG interaction, G-actin was functionalized on both sides of the bead. For GF interaction, G-actin was on the probe bead and F-actin was on the target bead. (C) AFM; GG (left) and GF (right) interactions. For GG interaction, G-actin was functionalized on the petri dish and the cantilever. For GF interaction, G-actin was on the cantilever and F-actin was on the petri dish.

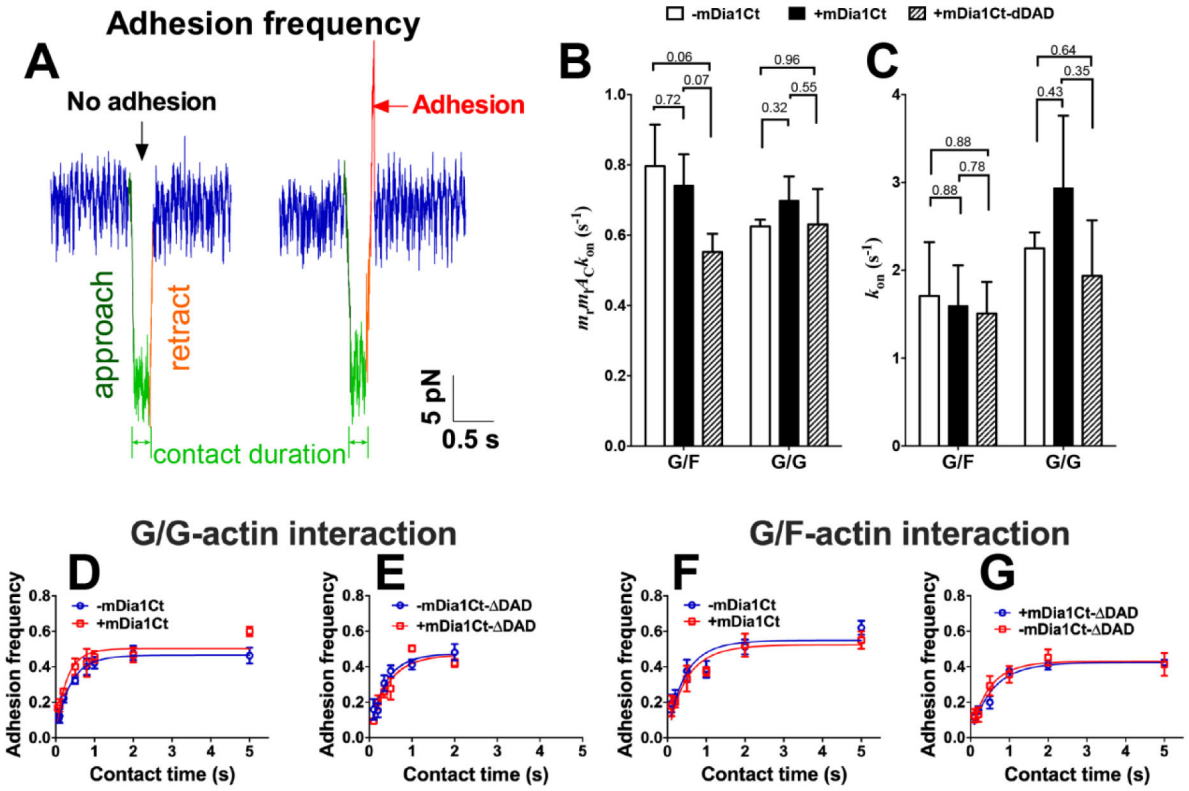

FIGURE 2.

Force-free kinetics of GG and GF interactions. (A) Time-force traces without (*left*) and with (*right*) a binding event but no bond lifetime. Green traces represent contact between the two bead surfaces. The horizontal length of the trace is the contact duration. Blue traces represent base-line signal without applied force. Red traces represent force signals that start with a linear ramp of force increase. The bond was loaded with a force until dissociation. (B and C) Force-free kinetic rates of GF and GG interactions in the presence and absence of formin, measured by BFP. (B) The product of molecular densities (m_r, m_1) and effective on-rates ($A_C k_{on}$). (C) Off-rates (k_{off}). Values were derived from fitting the adhesion frequency vs. contact time data (D to G) to a probabilistic binding model (Equation 1). The data points in the (D to G) were represented as mean ± SEM of 5 bead pairs with 50 measurements. Error bars represent a 95% confidence interval. The differences between values in each group are not significant as labeled in the figure ($P>0.05$, the unpaired Student's t-test between each pair). (D to G) Adhesion frequency measurement of GG (D and E) and GF (F and G) interaction in the absence (blue circle) or presence (red square) of mDia1Ct (D and F) or mDia1Ct-ΔDAD (E and G) at different contact times. Data are represented as mean ± SEM of 5 bead pairs with 50 measurements.. The on-rate and off-rate were obtained by fitting the curves (solid line) by probabilistic kinetics model for single-step monovalent receptor-ligand interaction (details in Experimental Procedures).

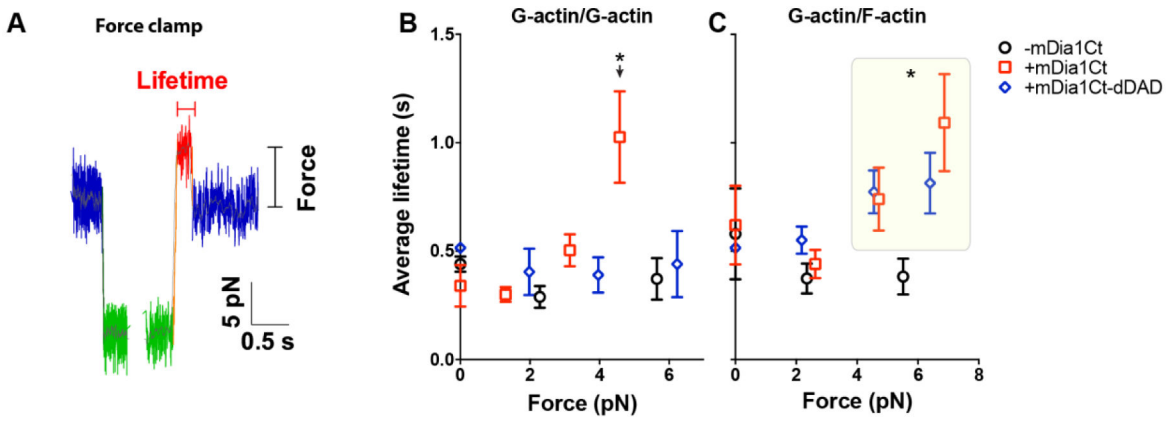

FIGURE 3.

Force-dependent lifetimes of GG and GF bonds in the presence or absence of formin, measured by BFP. (A) Representative time-force trace of a binding with lifetime event. Red traces represent force signals that start with a linear ramp followed by force-clamp at a constant level. The duration from the time clamped at a given force to bond rupture was measured as bond lifetime. (B and C) GG (B) and GF (C) interactions in the absence (black circle), and in the presence of mDia1Ct (red square) or mDia1Ct-ΔDAD (blue diamond). As force increases, the average bond lifetime significantly increases. Data are represented as mean ± SEM. 43 (2 pN) and 34 (5 pN) of measurements for GG without formin, 60 (1 pN), 98 (3 pN), 96 (5 pN) for GG with mDia1Ct, 28 (2 pN), 55 (4 pN), 75 (6 pN) for GG with mDia1Ct-ΔDAD. 98 (2 pN) and 126 (6 pN) of measurements for GF without formin, 55 (2 pN), 67 (5 pN), 79 (7 pN) for GF with mDia1Ct, 95 (2 pN), 93 (4 pN), 111 (6 pN) for GF with mDia1Ct-ΔDAD. All the measurements and the lifetime distributions are shown in in Fig. S1, Table 1 for the fitting to the distributions. * indicates statistical difference from others by the unpaired Student's t-test (arrow in the B and gray box in the C). See also Table S2 & S3 for the t-test statistical analysis between the average lifetime at different force level.

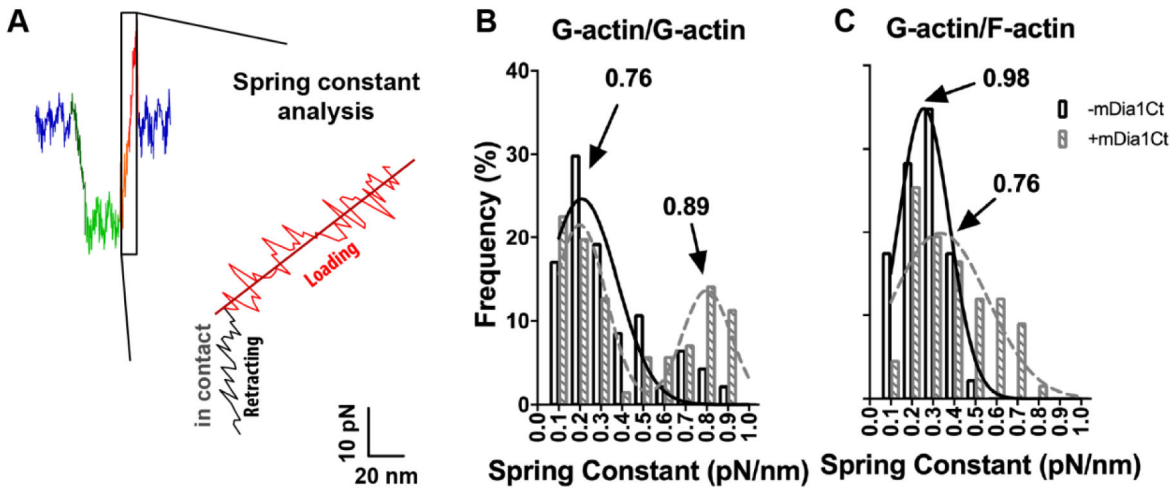

FIGURE 4.

Effects of formin association on the mechanical properties of GG and GF bonds, measured by BFP. (A) Force vs. displacement data obtained by combining data from the force vs. time in the ramping phase (red trace) with the date from displacement vs. time in capacitive feedback control sensor. The slope of the force-displacement trace represents the stiffness (spring constant) of the molecular complex. (B and C) Histogram of molecular spring constants of the GG (A; 46 measurements for −mDia1Ct and 67 measurements for +mDia1Ct) and GF (B; 49 measurements for −mDia1Ct and 71 measurements for +mDia1Ct) bonds in the presence (gray dashed) and absence (white bar) of mDia1Ct. The extra sum-of-squares F test was used to determine whether the single Gaussian or dual Gaussian is a better fit. The numbers in figures indicate the goodness-of-fit (R2).

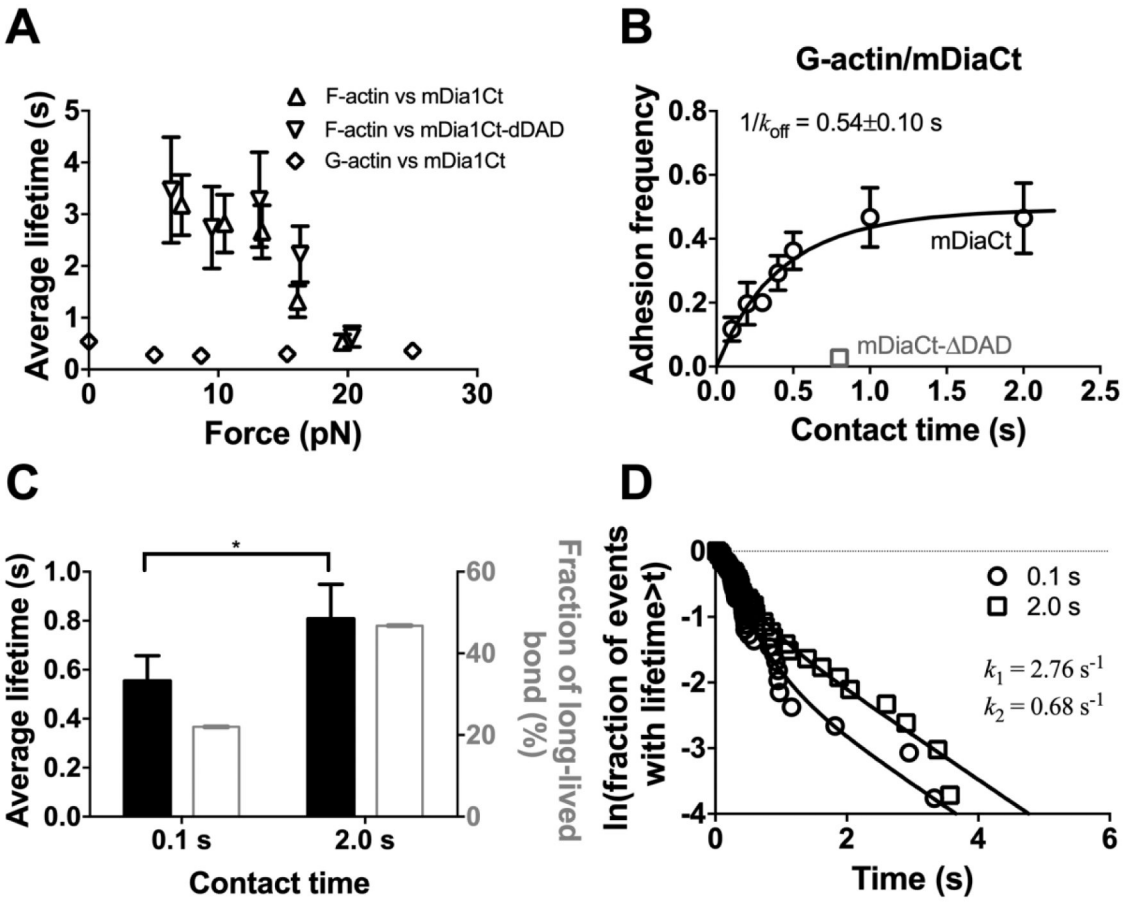

FIGURE 5.

Effects of force on formin-actin interactions. (A) Force-dependent lifetimes of mDia1Ct/F-actin (Δ), mDia1Ct-dDAD/F-actin (∇), and mDia1Ct/G-actin (◇) bonds, measured by AFM. Data are presented as mean ± SEM for each point. 62 (7 pN), 66 (10 pN), 70 (13 pN), 35 (16 pN) and 30 (20 pN) of measurements for mDia1Ct/F-actin. 36 (6 pN), 44 (10 pN), 54 (13 pN), 32 (16 pN) and 31 (20 pN) of measurements for mDia1Ct-dDAD/F-actin. 37 (5 pN), 97 (10 pN), 50 (15 pN) and 18 (20 pN) of measurements for mDia1Ct/G-actin. All the measurements are shown in the lifetime distributions in the Figure S4. The unpaired Student's t-test indicates no statistical difference ($p>0.05$) between the average lifetimes at the different forces for mDia1Ct/G-actin interaction. (B) Adhesion frequency versus contact time plot of mDia1Ct/G-actin interaction, measured by BFP. Data (circles, Mean ± SEM of 5 bead pairs) were fitted using Equation 1 (curve) to obtain force-free $A_c k_{on}$ and k_{off}. Gray square represents measurements of mDiaCt-ΔDAD/G-actin at a fixed contact time interaction (3 beads pairs with 50 contacts for each). (C and D) The effect of contact duration on GG interaction in the presence of mDia1Ct, measured by BFP. (C) The average bond lifetimes (open bars; left Y-axis) and the fraction of long-lived bond (striped gray bars; right Y-axis) with 0.1- or 2-s contact time. Data are represented as mean ± SEM of 43 and 41 measurements for 0.1 s and 2.0 s respectively. Error bars of the fraction represent a 95% confidence interval. (D) Bond lifetime distributions with different contact times, 0.1 s (circle) and 2 s (square). Solid lines are two-state model fits each of which consists of a

short- and long-lived state. The same k_1 (off-rate of short-lived state) and k_2 (off-rate of long-lived state) were used to fit both distributions, which were allowed to have different long-lived fractions.

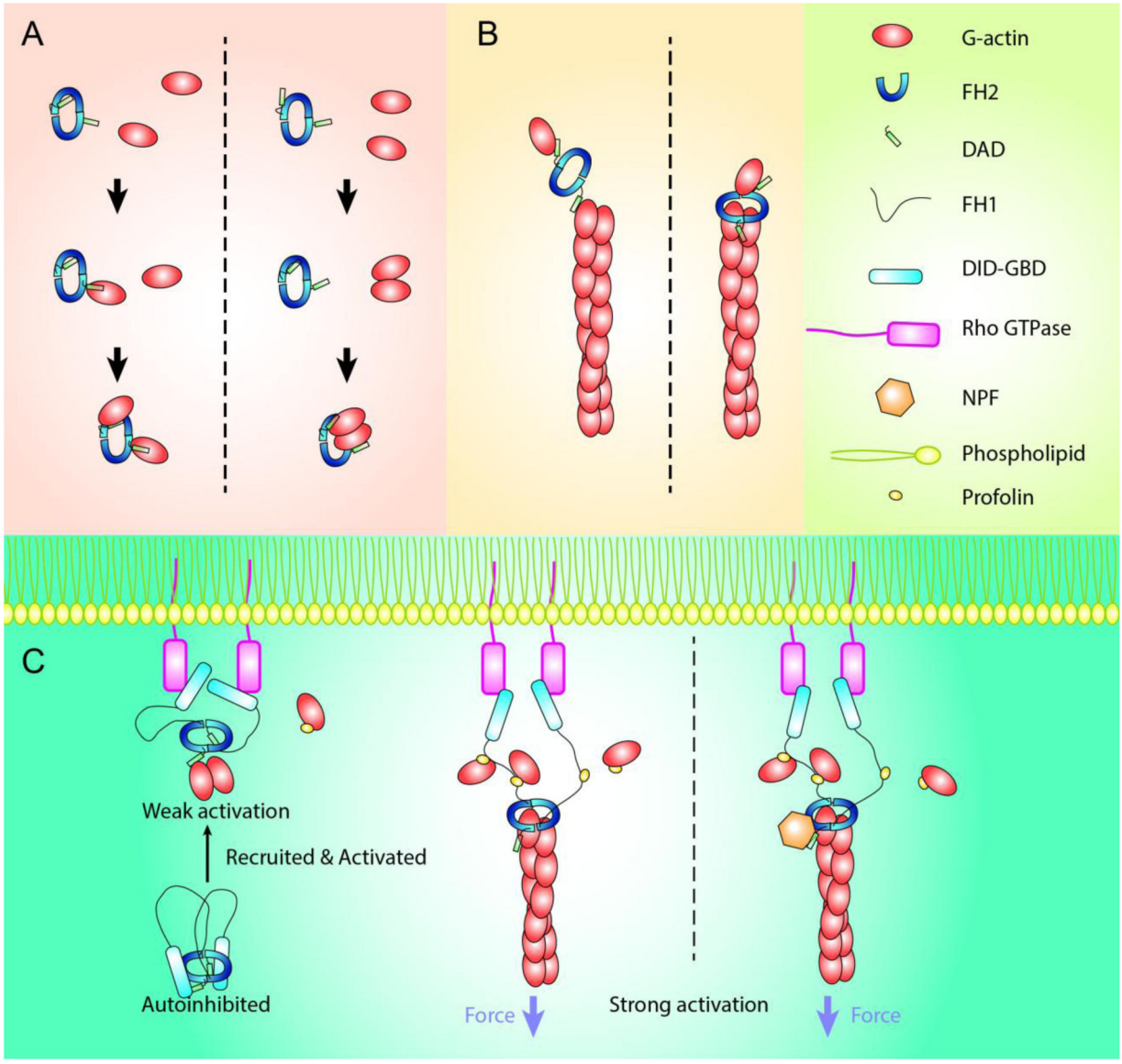

FIGURE 6.

Models for the integrated regulation of mDia1-mediated actin polymerization. (A) Two possible models of actin nucleation in the presence of formin. (*left*) Serial bond model. Actin nucleation is initiated by forming a series of bonds consisting of a DAD/G-actin bond, the flexible tether linking the two DAD domains in the FH2 dimer, and another DAD/G-actin bond. The association rate between two G-actin coated surfaces is expected to increase in the presence of formin. (*right*) Compact tetramolecular complex model. Two actin monomers spontaneously dimerize; the formin dimer embraces the actin dimer; and the stabilized molecular complex promotes further actin assembly. The association rate between two G-actin coated surfaces is not expected to increase in the presence of mDia1Ct. When tensile force is loaded on the complex, the actin dimer is further stabilized. (B) Two possible models of F-actin elongation in the presence of formin. (*left*) Serial bond model. Addition of an actin monomer to the barbed end of an actin filament is mediated by a FH2 dimer where

one of the DAD domain interacts with the G-actin and the other DAD domain interacts with the F-actin. (*right*) Compact complex model. A FH2 dimer caps the barbed end of F-actin. (C) Model of formin activation and function, with force playing an important role as a nucleation and activation promoting factor (NPF). The autoinhibited mDia1 is recruited to the plasma membrane and weakly activated through interaction with RhoA, phospholipid and local G-actins. Interaction with NPFs, increase in local G-actin concentration and force loading further activate formin. Figure 6C was adapted from Maiti, S., et al. (2012) [13].

Table 1.

Parameter values obtained by fitting lifetime distributions under force-loading conditions in the absence and presence of mDia1Ct.

The curves in Figure S1 were fitted by a single- or two-state dissociation model. Three parameters are used to fit two-state dissociation model, k_1, k_2, and α (details in Experimental Procedures). k_1, is off-rate of short-lived, k_2 is off-rate of long-lived state and α is the occupancy of long-lived bond. The off-rate from single-state dissociation fitting is also indicated as k_1 for the sake of comparison. The values in parentheses are reciprocal of k, a theoretical average lifetime of the bond state. α values are between 0 and 1.

G/G	**−mDia1Ct**		**+mDia1Ct**			**+mDia1Ct–ΔDAD**		
Force	**2 pN**	**5 pN**	**1 pN**	**3 pN**	**5 pN**	**2 pN**	**4 pN**	**6 pN**
k_1 (s^{-1})	2.64	1.46	3.59	4.96	4.19			
k_2 (s^{-1})	-	-	-	0.85	0.27			
α	0	0	0	0.34	0.26			
G/F	**−mDia1Ct**		**+mDia1Ct**					
Force	**2 pN**	**6 pN**	**2 pN**	**5 pN**	**7 pN**	**2 pN**	**4 pN**	**6 pN**
k_1 (s^{-1})	1.6	11	1.8	4.0	6.0	1.5	0.96	8.6
k_2 (s^{-1})	-	0.51	-	0.46	0.32	-	-	0.45
α	0	0.18	0	0.30	0.35	0	0	0.36